Combination drug screen targeting glioblastoma core vulnerabilities reveals pharmacological synergisms

Jérémy Ariey-Bonnet,[a,i] Raphael Berges,[b] Marie-Pierre Montero,[a] Baptiste Mouysset,[a] Patricia Piris,[a] Kevin Muller,[a] Guillaume Pinna,[c] Tim W. Failes,[d,e] Greg M. Arndt,[d,e] Philippe Morando,[b] Nathalie Baeza-Kallee,[b] Carole Colin,[b] Olivier Chinot,[f] Diane Braguer,[b] Xavier Morelli,[a] Nicolas André,[a,g,h] Manon Carré,[a] Emeline Tabouret,[b,f] Dominique Figarella-Branger,[b] Marion Le Grand,[a,**] and Eddy Pasquier[a,h,*]

[a]Aix Marseille Université, Centre National de la Recherche Scientifique (CNRS), Institut National de la Santé et de la Recherche Médicale (INSERM), Institut Paoli Calmettes, Centre de Recherche en Cancérologie de Marseille (CRCM), Marseille, France
[b]Aix Marseille Université, CNRS, UMR 7051, INP, Inst Neurophysiopathol, Marseille, France
[c]Institute for Integrative Biology of the Cell (I2BC), CEA, CNRS, University Paris-Sud, Université Paris-Saclay, Gif-sur-Yvette F-91198, France
[d]Children's Cancer Institute, Lowy Cancer Research Centre, UNSW Sydney, Sydney, NSW 2052, Australia
[e]ACRF Drug Discovery Centre for Childhood Cancer, Children's Cancer Institute, Lowy Cancer Research Centre, UNSW Sydney, Sydney, NSW 2052, Australia
[f]Aix-Marseille University, Assistance Publique-Hopitaux de Marseille, Centre Hospitalo-Universitaire Timone, Service de Neuro-Oncologie, Marseille, France
[g]Pediatric Oncology and Hematology Department, Hôpital pour Enfant de La Timone, AP-HM, Marseille, France
[h]Metronomics Global Health Initiative, Marseille 13385, France

eBioMedicine
2023;95: 104752
Published Online xxx
https://doi.org/10.1016/j.ebiom.2023.104752

Summary

Background Pharmacological synergisms are an attractive anticancer strategy. However, with more than 5000 approved-drugs and compounds in clinical development, identifying synergistic treatments represents a major challenge.

Methods High-throughput screening was combined with target deconvolution and functional genomics to reveal targetable vulnerabilities in glioblastoma. The role of the top gene hit was investigated by RNA interference, transcriptomics and immunohistochemistry in glioblastoma patient samples. Drug combination screen using a custom-made library of 88 compounds in association with six inhibitors of the identified glioblastoma vulnerabilities was performed to unveil pharmacological synergisms. Glioblastoma 3D spheroid, organotypic *ex vivo* and syngeneic orthotopic mouse models were used to validate synergistic treatments.

Findings Nine targetable vulnerabilities were identified in glioblastoma and the top gene hit *RRM1* was validated as an independent prognostic factor. The associations of CHK1/MEK and AURKA/BET inhibitors were identified as the most potent amongst 528 tested pairwise drug combinations and their efficacy was validated in 3D spheroid models. The high synergism of AURKA/BET dual inhibition was confirmed in *ex vivo* and *in vivo* glioblastoma models, without detectable toxicity.

Interpretation Our work provides strong pre-clinical evidence of the efficacy of AURKA/BET inhibitor combination in glioblastoma and opens new therapeutic avenues for this unmet medical need. Besides, we established the proof-of-concept of a stepwise approach aiming at exploiting drug poly-pharmacology to unveil druggable cancer vulnerabilities and to fast-track the identification of synergistic combinations against refractory cancers.

Funding This study was funded by institutional grants and charities.

Keywords: Drug combination screening; Target deconvolution; Pharmacological synergisms; Glioblastoma; Cancer vulnerabilities

*Corresponding author. Aix Marseille Université, Centre National de la Recherche Scientifique (CNRS), Institut National de la Santé et de la Recherche Médicale (INSERM), Institut Paoli Calmettes, Centre de Recherche en Cancérologie de Marseille (CRCM), Marseille, France.
**Corresponding author.
E-mail addresses: eddy.pasquier@inserm.fr (E. Pasquier), marion.le-grand@inserm.fr (M. Le Grand).
[i]Current address: Biotech Research & Innovation Centre, University of Copenhagen, 2200 Copenhagen N, Denmark.

Research in context

Evidence before this study

Despite significant advances in the understanding of glioblastoma biology in recent years, no major breakthrough has been translated into the clinic yet. The standard-of-care has been solely based on radiotherapy in combination with Temozolomide chemotherapy for more than 15 years. Despite intensive treatments, median survival of glioblastoma patients is approximately 15 months and less than 7% survive 5 years after diagnosis. In this context, combination therapy is an attractive strategy since the association of two drugs can be synergistic and thus allow better anti-tumor response with lower concentration of single agents. However, with more than 5000 approved-drugs and compounds in clinical development, pinpointing pharmacological synergisms represents a major technical challenge.

Added value of this study

We provide proof-of-concept of the efficacy of a multi-modal chemogenomic screening approach to reveal and therapeutically exploit cancer core vulnerabilities. This methodology was applied to glioblastoma, leading to the identification of nine targetable vulnerabilities: RRM1, PLK1, CHK1, AURKB, CDK1, AURKA, mTOR, HDAC3 and ATP1A1. We validated the major role of RRM1 in glioblastoma spheroid growth and demonstrated that it constitutes an independent prognostic marker using glioblastoma patient biopsies. Furthermore, we highlighted synergistic drug combinations, including the associations of CHK1 and MEK inhibitors as well as AURKA and BET inhibitors against glioblastoma spheroid models. These drug combinations have been previously documented in other studies but their identification in our high-throughput screening approach and validation in clinically-relevant models of glioblastoma considerably strengthen the level of evidence of their efficacy. In particular, we provide the validation in an original *ex vivo* organotypic and an orthotopic syngeneic mouse models of the therapeutic potential of the dual AURKA/BET inhibition against glioblastoma.

Implications of all the available evidence

Our work opens new therapeutic avenues for glioblastoma patients. Given that Alisertib and Birabresib have been already tested in phase I clinical trial, the therapeutic potential of the dual AURKA/BET inhibition could be rapidly translated to the clinic. Our results also point out the interest of developing RRM1 inhibitors that can effectively cross the blood brain barrier for glioblastoma treatment. Importantly, all the datasets generated in our study, including our dual drug and RNAi screening, are available to the scientific community. This could appeal to clinicians and scientists working on glioblastoma biology and provide rationale for translational projects focusing on identifying pharmacological synergisms. Lastly, our stepwise method could be applied to other refractory cancers, thus paving the way for therapeutic interventions in unmet medical needs.

Introduction

Next generation sequencing has revolutionized our understanding of the molecular pathways that drive the development and progression of human cancers.[1] The establishment and expansion of large-scale cancer databases have allowed scientists to mine and analyze an unprecedented number of patient-derived datasets that could lead to the identification of targetable vulnerabilities.[2] Nonetheless, translation of these major findings into clinical practice has been slower than expected. This could be partly explained by the current dominant paradigm in drug discovery based on the identification of one specific disease-related target leading to the design of selective inhibitors/activators of this target. However, it is now well-established that most effective drugs act on multiple rather than single targets and combination therapy is the most effective strategy to treat complex diseases, such as cancers.[3,4] In this context, drug polypharmacology could open major therapeutic avenues.[5–7] The number of possible combinations being almost infinite, data-driven approaches to find optimal treatments are needed. Here, we hypothesized that screening existing drugs (either already-approved or in clinical development) associated with target deconvolution represent a unique opportunity to exploit drug polypharmacology for the identification of core vulnerabilities in cancer. Those targets can then be used to rationally design biology-driven drug combination screens to find synergistic treatments.

Gliomas are the most common primary brain tumors in neuro-oncology practice of adults.[8] About half of all newly diagnosed gliomas is classified as glioblastoma (GBM), which is the most malignant type of brain cancer defined as grade 4 in the 2021 World Health Organization Classification.[8] More than 90% of all cases are classified as primary tumors that arise *de novo*. GBM were previously classified into four subtypes based on transcriptional features: classical, proneural, mesenchymal and neural. However, integrating the malignant cell programs, their plasticity and their modulation by genetic drivers as well as certain molecular markers, including TERT promoter mutation, IDH1/2 mutation, *MGMT* promoter methylation or the combination of whole chromosome 7 gain/10 loss, demonstrates the high inter-patient and intratumor heterogeneity and can now provide powerful prognostic information.[9,10]

Median patient survival is approximately 15 months and less than 7% of patients survive 5 years after diagnosis, contributing to 3–4% of all cancer-related deaths worldwide.[11] Despite recent advances in our understanding of glioma biology, the current standard-of-care for GBM is still based on tumor resection with concurrent radiotherapy and chemotherapy with temozolomide.[11] Nevertheless, in the majority of cases, acquired resistance to both radiation and temozolomide occurs. There is an urgent need to establish innovative strategies and discover new treatments to improve the outcome of patients with GBM.

In this study, we applied a chemogenomic screen targeting core vulnerabilities in GBM in order to quickly identify synergistic combinations. We uncovered that dual inhibition of BET proteins and aurora kinase A is highly synergistic against GBM using 3D spheroid, organotypic *ex vivo* and syngeneic orthotopic mouse models. Altogether, our study provides strong pre-clinical evidence of the dual AURKA/BET inhibition against GBM. Moreover, our work indicates that exploiting core vulnerabilities to design biology-driven drug screens represents a valuable strategy to discover highly synergistic drug combinations for refractory cancers.

Methods

Cell culture

The human GBM cell lines T98G (RRID: CVCL_0556), U87 (RRID: CVCL_0022) and its EGFR-mutated derivative U87vIII (RRID: CVCL_XZ66) were kindly provided by the Children's Cancer Institute (Sydney, Australia) while the murine GL261 (RRID: CVCL_Y003) GBM cell line was obtained from the German Collections of Micro-organisms and Cell Cultures (DSMZ, Germany; #ACC802). They were grown in Dulbecco's Modified Eagle Medium (Gibco, #11960044) containing 10% Fetal Calf Serum, 1% sodium pyruvate (Gibco, #11360070) and 1% penicillin-streptomycin (Gibco, #15140122). Fluorescently-labelled U87 and GL261 cell lines were established by transfection of an mtDsRed plasmid with Lipofectamine 2000 (Invitrogen, #11668019) according to the manufacturer's protocol, followed by geneticin selection (0.8 mg/ml, Gibco, #10131035) and two cycles of fluorescence-activated cell sorting. All cell lines were regularly screened and are free from mycoplasma contamination (Eurofins Genomics). We also used human primary GBM-initiating cells, mesenchymal-like GBM6 and proneural-like GBM9, previously established from two different human GBM tumor samples, characterized in our laboratory and transfected to stably express GFP.[12,13] These cells were grown in serum-free medium supplemented with a cocktail of optimized growth factors including EGF and bFGF (Peprotech #100-15a and #100-18b) as previously described.[12] All cell cultures were maintained in a humid atmosphere at 37 °C with 5% CO_2.

Drugs and reagents

Alisertib (10 mM, Selleckchem. #s1133), Birabresib (10 mM, Selleckchem. #s7360), Prexasertib (10 mM Selleckchem. #s6385), Mirdametinib (10 mM Selleckchem. #s1036), Panobinostat (10 mM Selleckchem. #s1030), Molibresib (10 mM Selleckchem. #s7189) and LY3295668 (10 mM Selleckchem. #s8782) were resuspended in dimethyl sulfoxide (DMSO, Sigma, #D5879). Stock solutions were stored at −20 °C. The solutions were diluted in culture medium extemporaneously for the experiments. All drugs used in our custom-made library were suspended in DMSO (Sigma, #D5879) and stock solutions were stored at −20 °C (Table S1 for details).

High-throughput drug screening

Three libraries (Prestwick chemical, Lopac and Tocris) containing ~2800 unique Federal Drug Administration (FDA)-approved drugs and pharmacologically-active molecules were screened in a primary screen on U87 cells at a single dose of 5 μM in triplicate. Cell viability was assessed after 72 h incubation using a home-made Alamar Blue solution (75 mg resazurin (Sigma, #R7017), 12.5 mg methylene blue (Sigma, #M9140), 164.5 mg potassium hexacyanoferrate III (Sigma, #P8131) and 211 mg potassium hexacyanoferrate II trihydrate (Sigma, #P9387), 500 ml water) as previously described.[14] Assay performance was evaluated by calculating the Z-factor for each assay plate, according to the method described by Zhang et al.[15] Compounds were considered candidates when they significantly inhibited cell viability by at least 50%. The top 280 candidates were screened in the U87, its EGFR-mutated derivative U87vIII, and T98G cell lines, using the same methodology. Compounds were defined as confirmed hits when they significantly inhibited cell viability by at least 50% in 2 out of the 3 tested GBM cell lines.

Focused siRNA library generation

All the known targets and interactors of the pharmacological hits were listed by interrogating three complementary databases: DrugBank (RRID: SCR_002700 https://go.drugbank.com/), Gostar (https://www.gostardb.com/gostar/) and DRUGSURV.[16] This yielded a total of 1100 known targets and interactors, of which 292 were associated with at least 3 pharmacological hits. A focused siRNA library (Silencer™ Select pre-designed siRNA; ThermoFisher Scientific) was designed to individually silence the genes encoding the 292 targets/interactors, with 3 different and specific siRNA sequences per gene.

High-throughput siRNA screening

For screening purpose, an automated reverse transfection protocol was developed on a robotic workstation equipped with a 96-well head probe (Nimbus,

Hamilton). Each siRNA sequence from the library was transfected as a separate triplicate in different well positions of 3 independent culture plates to minimize positional errors. Each culture plate also received different positive and negative controls. Eight wells received the transfection reagent alone ("MOCK" well, negative control), 16 were transfected with a scrambled siRNA ("NEG" wells, negative control, Ambion), and 8 were transfected with a pool of cytotoxic siRNAs ("All-Stars" wells, positive control, Allstars maximal death control, Qiagen). Briefly, siRNA sequences were lipoplexed with Lipofectamine RNAiMAX (Life Technologies, #13778150) in clear bottom, black-walled 384-well culture plates (Greiner μClear plates, #781091). After 15 min of complexation, GBM cell lines were seeded on top of the lipoplexes (1000 cells/well; final [siRNA] = 5 nM) and incubated for 3 days at 37 °C and 5% CO_2 in a humidified incubator. Cells were fixed with Paraformaldehyde 4% (Sigma, #1004969011), stained with Hoechst 33342 and plates were imaged on a High-Content Imaging device (Operetta HCS epifluorescence microscope, PerkinElmer). Three fields per well were acquired at 10× magnification in blue channel (excitation: 380 ± 20 nm; emission: 445 ± 35 nm). Hoechst-stained nuclear regions of interest were segmented using Harmony software (RRID: SCR_023543 PerkinElmer) and cell viability was expressed in each plate as the relative number of cellular events in sample wells relative to the average of NEG wells. Genes were considered as candidates when at least 2 out of 3 siRNA sequences gave statistically significant results in at least 2 GBM cell lines (Z-score scoring). Candidate genes were retested in an identical setup, and genes were accepted as hits when they passed the selection criteria (2/3 active siRNA sequences) a second time and leading to at least 20% of decrease in cell viability in all tested cell lines.

DepMap database analysis

Using the Dependency Map portal (RRID: SCR_017655 https://depmap.org/portal/), we extracted from the CRISPR DepMap 22Q2 Public + Score, Chronos dataset, the gene effect scores derived from CRISPR knockout screens published by Broad's Achilles and Sanger's SCORE projects. Gene effect scores were inferenced by Chronos (https://genomebiology.biomedcentral.com) and integration of the Broad and Sanger datasets was performed as described in Pacini et al.,[17] except that quantile normalization was not performed. Negative scores imply cell growth inhibition and/or death following gene knockout. Scores are normalized such that non-essential genes have a median score of 0. As a criterion, genes were considered hits when their gene effect scores are <–0.5 in all 3 selected GBM cell lines (U87MG, U251 and T98G — DepMap id: ACH-000075, ACH-000232 and ACH-000571 respectively).

Functional validation assay

The EGFR-mutated derivative model of U87, U87vIII and mtDsRed-expressing U87 cell lines were seeded in T25 cell culture flasks with 4 ml medium and transfected with 1 ml of Opti-MEM medium (Gibo, #11058021) containing 1% of lipofectamine RNAiMax (Life Technologies, #13778150) and 5 nM of siRNA. Three different siRNA sequences targeting *RRM1* (Silencer® Select #s12357, #s12358, #s12359; ThermoFisher Scientific) were used as well as a non-targeting negative control siRNA with no significant sequence homology to mouse, rat or human gene sequences (Silencer® Select #AM4635). Two days later, cells were seeded in 96-well U bottom and low-binding plates in DMEM medium containing methylcellulose at 0.6 g/L. Spheroid growth was evaluated either daily for one week by measuring the fluorescence ratio (575 nm: excitation wavelength/620 nm: emission wavelength) in the case of mtDsRed expressing U87 cells or after 8 days by Alamar Blue in the case of U87vIII cells. Both measurements were performed with a PHERAstar® plate reader (BMG). To evaluate the level of gene knock-down, cells were harvested 48 h after transfection and total RNA was extracted using RNeasy Plus mini kit (Qiagen, #74136), following the manufacturer's instructions. Reverse transcription was performed with Onescript® cDNA synthesis kit (Abm, #G236) and qRT-PCR was undertaken using SsoAdvanced Universal SYBR® Green Supermix (Bio-Rad) and a CFX96™ Real-Time System device (Bio-Rad). Gene expression level of *RRM1* was determined using the $\Delta\Delta C_t$ method, normalized to the *YWHAZ* or *GAPDH* control genes. The following predesigned KiCqStart SYBR® Green primers (Merck, Fontenay-sous-bois, France) were used.

- *RRM1* (forward: 5′-CATTGGAATTGGGGTACAAG; reverse: 5′- AATTCCTTTGCTAACTGGAG),
- *GAPDH* (forward: 5′-ACAGTTGCCATGTAGACC reverse: 5′- TTTTTGGTTGAGCACAGG) and
- *YWHAZ* (forward:5′-AACTTGACATTGTGGACA TC; reverse: 5′AAAACTATTTGTGGGACAGC).

To evaluate the level of protein knockdown, cells were lysed in RIPA buffer (Tris–HCl 50 mM pH 8.0, NaCl 250 mM, Triton-X100 0.1%) freshly supplemented with a cocktail of protease and phosphatase inhibitors (Sigma–Aldrich, #PPC2020), 72 h after siRNA transfection. Protein concentrations were determined using the Bio-Rad Protein Assay (Bio-Rad, #5000001). Proteins were separated by SDS-PAGE and electro-transferred onto a nitrocellulose membrane. Primary antibodies were directed against RRM1 (clone EPR8483; Abcam, #ab137114) and α-tubulin (clone DM1A; Sigma Aldrich; RRID: AB_310035). Peroxydase-conjugated secondary antibodies (Cell Signaling, #7074; RRID: AB_2099233 and #7076; RRID: AB_330924) and chemiluminescence detection kit (Millipore) were used for visualization with

ChemiDoc Touch Imaging System (BioRad). Membranes were probed again with α-tubulin antibody following a step of stripping using a solution of 5% trichloroacetic acid.

Gene expression analysis on patient samples

Gene expression analysis was conducted using the R2 microarray analysis and visualization platform (http://r2.amc.nl). RNA-seq data were extracted from two independent cohorts providing open access to data acquired from various forms of cancer, The Cancer Genome Atlas (TCGA) database, and from normal tissues, the Genotype-Tissue Expression (GTeX) database. GBM TCGA dataset was used and partitioned in five subtypes according to the data available: classical (n = 17), mesenchymal (n = 27), neural (n = 17), proneural (n = 24) and not determined (n = 455). We used GTeX normal brain tissue data from the following subgroups: caudate (n = 246), cortex (n = 255), frontal cortex (n = 209), nucleus accumbens (n = 246), putamen (n = 205), spinal cord (n = 159) and thalamus (n = 202). Median values of *RRM1, BRD2, BRD3, BRD4* and *AURKA* were recorded using log2 transformation gene expression. Statistical analyses using ANOVA were performed to compare GBM subtypes gene expression to normal brain tissue gene expression. Boxplots were generated using GraphPad Prism 9.4.1 (RRID: SCR_002798).

Protein expression analysis on patient samples

Ninety-seven patients (n = 33 females and n = 64 males) were included in this study and all patient samples were coming from primary GBM. They had histologically confirmed GBM, *IDH*-wt,[18] were between the age of 33–75 (median 60.5), were not included in experimental therapeutic protocols and were homogeneously treated by the Stupp protocol (Temozolomide + radiotherapy). Tissue microarrays (TMA) were constructed from routinely processed formalin-fixed paraffin-embedded tumor material. Areas of viable and representative tumor following review of all blocks were marked by a pathologist (Pr Figarella-Branger) prior to inclusion into the TMA (3 × 0.6 mm cores for each tumor). Immunohistochemistry study was performed on TMA. After steam-heat induced antigen retrieval, 5 µm sections of formalin-fixed paraffin-embedded samples were tested for the presence of RRM1 (Rabbit monoclonal, clone EPR8483; Abcam). A Benchmark Ventana autostainer (Ventana Medical Systems SA, Illkirch, France) was used for detection and TMA slides were simultaneously immunostained in order to avoid inter-manipulation variability. Immunostaining was scored in blind by a pathologist (Pr Figarella-Branger), analyzing for each triplicate the core demonstrating the strongest immunoreaction, and using the immunoreactive score (IRS) previously described by Casar-Borota et al.[19]; the IRS (0–12) being the product of the proportion of immunoreactive cells (0, 0%; 1, <10%; 2, 10–50%; 3, 51–80% or 4, >80%) and the staining intensity (0, no staining; 1, weak; 2, moderate and 3, strong). The Kaplan–Meier method was used to estimate survival distributions. Log-rank tests were used for univariate comparisons. Cox proportional hazards models were used for multivariate analyses and for estimating hazard ratios in survival regression models. Multivariate analysis included extent of surgical resection. All the tests were two-sided and $p < 0.05$ was considered significant for each statistical analysis. Statistical analyses were conducted using the PASW Statistics version 17 (IBM SPSS Inc., Chicago, IL, USA).

Drug combination screening

Briefly, 4000 living cells from the GL261 murine GBM cell line were seeded per well with the Certus Flex® (GyGer) in 384-well plates (Corning, #3830). Cells were incubated in the presence of a custom-made drug library containing 88 drugs alone (Table S1 for details) or in association with Alisertib 1 µM, Prexasertib 10 nM, Vistusertib 250 nM, Dinaciclib 5 nM, Rigosertib 250 nM or Panobinostat 10 nM. Drugs were distributed with the Echo 550 liquid dispenser® (Labcyte) at 6 different concentrations covering 3 logs (*i.e.*, 1 nM–1 µM, 10 nM–10 µM or 100 nM–100 µM) in constant DMSO. Cell viability was measured using CellTiter-Glo® 2.0 Cell Viability Assay (Promega, #G9243) after 72 h of drug incubation in a humidified environment at 37 °C and 5% CO2. Luminescence was measured using a PHERAstar® plate reader (BMG). Data were normalized to negative control wells (DMSO only). IC_{50}, defined as half maximal inhibitory concentration values, and AUC (Area Under the dose response Curve — %.mol.L^{-1}) were obtained using library (ic50), library (drc), library (ggplot2) and library (PharmacoGx) packages from R studio.

3D spheroid cell viability assay

The mtDsRed-expressing U87 and GL261 GBM cells were seeded at 2000 and 4000 cells/well, respectively, while the GBM6 and GBM9 cell lines were seeded at 1000 cells/well in 96-well U bottom low-binding plates in DMEM medium containing methylcellulose (0.3 g/L). After 1 and 6 days for the GL261 and U87 cells and after 3 and 6 days for the GBM6 and GBM9 cells, spheroids were treated with a 6 × 5 combination matrix containing two compounds at different concentration ratios. After 10 days of treatment for the GBM6 and GBM9 models, cell survival was detected by addition of Cell Titer Glo® (Promega, #G9682), while metabolic activity was detected by addition of Alamar blue after 15 days of treatment in GL261 and U87 spheroids, using a PHERAstar® plate reader (BMG). Cell viability was determined and expressed as a percentage of untreated control cells. To assess the synergy score of the tested combinatorial treatments, Bliss heatmaps were generated using the

SynergyFinder web application (https://synergyfinder.fimm.fi).[20]

Microscope image acquisition

Images of U87vIII and mtDsRed-expressing U87 spheroids were acquired by phase contrast and RFP fluorescence channel using a 4x/0.13 objective with an EVOS FL® Cell Imaging System (Invitrogen) and images of mtDsRed-expressing U87 and GL261 spheroids were acquired by RFP fluorescence channel using a 4x/0.1 objective with a Leica DM IL LED® (Leica) at the end point of experiments.

Brain organotypic model development and analysis

To establish organotypic cultures, the healthy brains of Swiss immunocompetent mice were surgically harvested and sectioned into thick slices using a vibrating blade microtome (RRID:SCR_016495). A 4-day spheroid formed from 4000 mtDsRed-expressing GL261 cells or a 2-day spheroid formed from 5000 GFP-expressing GBM6 cells was grafted onto each brain slice. These organotypic co-culture models were placed on inserts with 0.4 µm pore size membranes (Falcon®, #353090) and maintained in medium containing 50% MEMa, 25% horse serum (Gibco, #16050122), 25% Hanks' Balanced Salt Solution (HBSS; Gibco, #14065056), 10 mM HEPES buffer (Gibco, #15630106), 28 mM Glucose (Gibco, #15023021), 1% L-Glutamine (Gibco, #25030081) and 1% penicillin-streptomycin. Organotypic co-culture models were daily exposed to Alisertib (100 nM for GBM6 or 2.5 µM for GL261), Birabresib (500 nM for GBM6 or 1 µM for GL261) or their combination for 5 consecutive days. Tumor growth of mtDsRed-expressing GL261 cells within the brain slices was analysed over time using the JuLI™ Stage imaging system and the PHERAstar® plate reader (λ_{ex} 580nm/λ_{em} 620 nm–fluorescence signal acquisition with a 15 × 15 matrix scanning mode). Images of GFP-expressing GBM6 cells grafted into brain slices were acquired using a Zeiss AXIO-Observer Z1 microscope (Carl Zeiss SAS) with a 4 × fixed objective in the GFP+ channel. Images were automatically stitched together using the Tile Scan mode of the microscope. Area of each generated tumor was measured using ZEISS™ ZEN Software.

Animal study

Female C57BL/6 mice (6-weeks old; C57BL/6JOlaHsd subline) were obtained from Envigo company, France. They were anesthetized *via* intraperitoneal administration of a mixture of ketamine (100 mg/kg)/xylazine (10 mg/kg) and then placed in a stereotactic frame (Kopf) and a burr hole was drilled in the skull (1 mm anterior to bregma,—1 mm lateral). Fifty thousand murine GL261 GBM cells were inoculated in 2 µL of DMEM medium (0.5 µL/min) using a microliter Hamilton® syringe at 2 mm of the cortex surface, in the *corpus callosum*. Animals were observed until they fully recovered. Five mice were randomly housed per cage to ensure social interaction (365 × 205 × 140 cm, 530 cm^2). The housing conditions were: water and food ad libitum, temperature regulated at 22 ± 2 °C, day/night cycle 7:00 am-7:00 pm in winter and 8:00 am-8:00 pm in summer. Cages were placed in a ventilated cabinet. To guarantee the best possible animal welfare, the cages were enriched with nestlets and polycarbonate domes. Cages were changed and cleaned weekly. A total of 40 mice (single mouse being the experimental unit) was included in the study and randomized into 4 groups 1 week after tumor cell injection. The body weight and general status of mice were recorded every day. Mice were euthanized when they lost more than 20% of their initial body weight or displayed signs of distress or neurological deficits, and results were included in the study. Criteria used for excluding animals were injuries during experimental procedures, identified pathologies other than glioblastoma and mice fighting each other. Two mice were excluded of the study (one in the Alisertib alone group and another one in the drug combination group) due to an oral administration issue and injuries inflicted by other mice. Mice received oral administrations of Alisertib (25 mg/kg in 10 ml/kg application volume; n = 9 mice), Birabresib (75 mg/kg in 10 ml/kg application volume; n = 10 mice), Alisertib + Birabresib (25 mg/kg + 75 mg/kg in 10 ml/kg application volume, n = 9 mice), or vehicle only (10 ml/kg, vehicle groups, n = 10 mice) from day 7–28 after GBM implantation (5 administrations/week). Alisertib and Birabresib were resuspended in a mixture of DMSO (10%) and corn oil (90%—Sigma) to ensure full dissolution and achieve better gastrointestinal absorption of the drugs. Control group (vehicle only) was compared to each monotherapy and drug combination, which was also compared to monotherapies. Survival medians were estimated by the Kaplan–Meier product limit method. The log-rank test (Mantel–Cox test; significant with $p < 0.05$) was used to compare survival rates using GraphPad Prism 9.4.1 (RRID:SCR_002798). All data for this animal study are available at the Marseille Neurophysiology Institute (team 8), France.

Histology and immunohistochemical analysis

Serial 4-µm paraffin sections of brains were stained with hematoxylin and eosin and examined under the microscope for the presence of tumor cells. Immunohistochemistry was performed on adjacent paraffin sections with monoclonal anti-Ki67 (clone MIB-1; Dako; #GA626) and anti-cleaved-caspase 3 (Asp175; clone 5A1E; Cell Signaling; #9664; RRID:AB_2070042) antibodies using the avidin–biotin–peroxidase method (Vectastain Elite ABC kit, Vector Laboratories; #PK-6100).

Ethics

Patient tumor specimens for TMA were obtained according to a protocol approved by the local institutional review board and ethics committee (2014-A00585–42) and conducted according to national regulations. All the patients provided written informed consent. GBM formalin-fixed, paraffin-embedded (FFPE) samples provided by the AP-HM tumor bank (AC-2018-31053; CRB BB-0033-00097; DOI: http://doi.org/10.5334/ojb.63) were pooled on several home-made tissue microarrays for high-throughput screening. Brain explants for the organotypic models were obtained from the animal facility of the Faculty of Pharmacy, in accordance with the recommendations of the European Community (approval number: E 13 055 20). *In vivo* experiments were performed by adequately trained research personnel (Dr Berges and Mr Mouysset). The entire experimental protocol, including the research question, the key design features and the analysis plan, was prepared before the study through a project authorization request for ethics committee approval. The protocol was registered as number 2020030316384240, the document is archived in the offices of the Marseille ethics committee number 14 (authorization number #02201902). Researchers conducting the animal experimentations were aware of the group allocation at the different stages of the experiment. There was no blinding procedure applied.

Statistics

Each experiment was performed at least in triplicate. Data are presented as mean ± S.D or S.E.M as indicated in the figure legends. Statistical significance was tested using unpaired Student's t test. For experiments using multiple variables, statistical significance was assessed *via* two-way ANOVA. Log-rank (Mantel–Cox test) and Gehan-Breslow-Wilcoxon tests were used to compare animal survival by Kaplan–Meier analysis. A significant difference between two conditions was recorded for $*p < 0.05$; $**p < 0.01$; $***p < 0.001$. Figures were made using GraphPad Prism 9.4.1 (RRID: SCR_002798).

Role of funders

The funders did not have any role in study design, data collection, analysis, interpretation of data, writing of the manuscript or the decision to submit for publication.

Results

Stepwise chemogenomic screen identifies nine core vulnerabilities in GBM

To unveil disease-relevant targets through the exploitation of drug poly-pharmacology in GBM, we performed a high-throughput drug screen with three commercially available libraries containing small molecules that have well-annotated pharmacology and are suitable for phenotypic screens. More than 2800 unique already-approved drugs and pharmacologically active molecules (Table S2) were screened in the U87 GBM cell line and the top 280 primary candidates leading to a decrease of more than 50% of cell survival were selected and used in a secondary screen in the T98G, U87 and its EGFR-mutated derivative U87vIII cell lines (Table S3). Amongst the primary hits, 83 reduced the cell viability of at least 2 out of the 3 tested cell lines by more than 50% and were further confirmed as "GBM killers". Besides experimental drugs, which account for ~41% of the pharmacological hits (34/83), the high-throughput drug screen also identified 19 chemotherapy agents (~23%), 3 targeted therapies and 27 non-oncology drugs, of which 15 are FDA-approved drugs currently used for human diseases and could potentially be repurposed for the treatment of GBM (Fig. 1a–b and Table S4 for details). As the second step of our methodology, we performed target deconvolution using three chemoinformatic databases (DrugBank, Drugsurv and Gostar) to exploit drug poly-pharmacology. All the known molecular targets and interactors of the 83 pharmacological hits were listed (Table S5). Amongst the 1100 identified interactors, 292 were associated with at least three pharmacological hits and were used to design a focused siRNA library containing three individual sequences for each of the 292 top targets. As a third step, a siRNA screening was performed in three GBM cell lines, resulting in the identification of 22 pharmacologically targetable hits that decreased the viability of all tested GBM cell lines by at least 20% (Fig. 1c and Table S6 for details). Finally, to prioritize targets, we cross-evaluated our siRNA screening results with the CRISPR loss-of-function screen data cohort from the Cancer Dependency Map Project (https://depmap.org). Nine of the 22 genes identified by our focused siRNA screen were defined as essential genes (gene effect score <–0.5) in all tested GBM cell lines: *RRM1, PLK1, CHEK1, AURKB, CDK1, AURKA, FRAP1, HDAC3* and *ATP1A1* (Fig. 1d and Table S7).

To ascertain the potential of our methodology to reveal core vulnerabilities in GBM, we focused our functional study on the top gene hit *RRM1*, which encodes for the catalytic subunit of an enzyme playing a key role in the production of deoxyribonucleotides for DNA replication.[21] A transient knockdown using three different siRNA sequences leading to a significant inhibition of RRM1 gene and protein expression (Fig. 2a–b, Student's t-test) resulted in a decrease in tumor spheroid growth, observed at day 5 and maintained until day 8. This was reflected by a significant drop in the U87 tumor spheroid growth of 70 ± 10%, 56 ± 16% and 72 ± 6% for the siRNA sequences #1, #2 and #3 in comparison to control, respectively ($p < 0.001$, Fig. 2c, Student's t-test). Similar results were obtained with the U87vIII cells, in which *RRM1* knockdown resulted in a 65–72% decrease in tumor spheroid viability after 8 days in comparison to control ($p < 0.001$, Figure S1a–c,

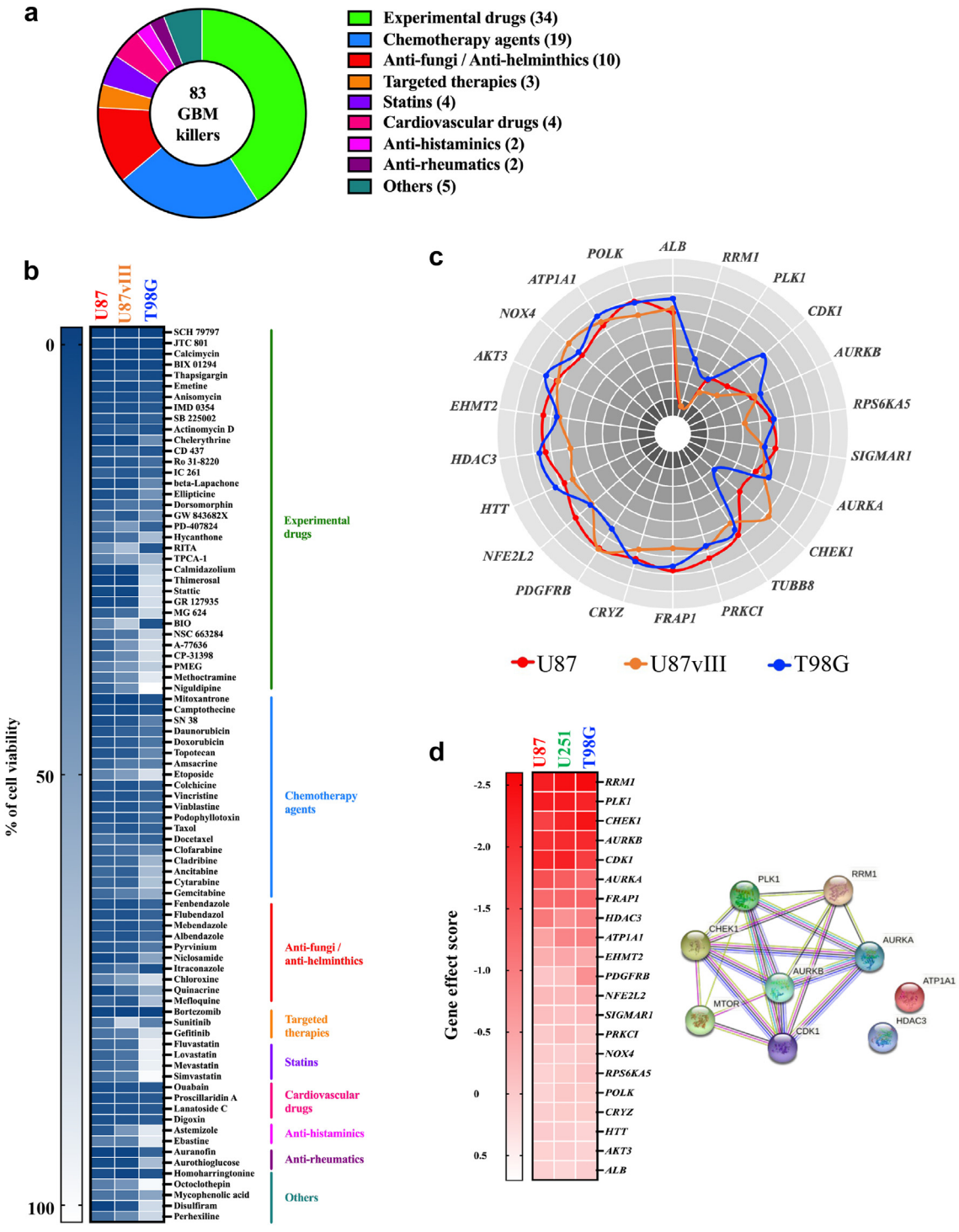

Fig. 1: **Stepwise chemogenomic screen identifies nine actionable gene vulnerabilities in GBM.** (**a**) Primary screen was performed in U87 GBM cell line with more than 2800 unique compounds tested alone (5 μM, n = 3 per condition from one experiment). After 72 h incubation, cell viability was assessed using Alamar Blue. The top 280 primary candidates were re-tested in a secondary validation screen in the T98G, U87 and its EGFR-mutated derivative U87vIII GBM cell lines using the same protocol. Eighty-three compounds were defined as GBM killers in at least 2 GBM cell lines and are represented in donut diagram and classified by pharmacological classes. (**b**) Heat map classification representing the cell viability in all tested GBM cell lines for the 83 hit compounds. (**c**) By target deconvolution using pharmacological online databases, 1100 known targets and interactors were

Student's t-test). Our transcriptomic analysis using freely available datasets in the R2 platform showed that *RRM1* expression is significantly up-regulated in GBM subtypes as compared to normal brain tissue (8.2 ± 0.2 and 3.3 ± 0.3, respectively; $p < 0.0001$; Figure S1d, ANOVA test). Furthermore, we evaluated RRM1 protein expression in primary GBM patient samples using immunohistochemistry staining of TMA (Fig. 2d). On the 97 analysed GBM samples, 69 cases (71%) were positive for RRM1 expression (24 cases were negative and 3 cases were not informative). We found that high expression of RRM1 (IRS from 4 to 12) was significantly associated with a poor outcome in univariate analysis ($p < 0.01$, Cox proportional hazards regression) and it remained prognostic in multivariate analysis (adjusted by type of surgery) ($p = 0.003$; HR = 1.991, 95% CI [1.259–3.147]). Altogether, these results demonstrate that our stepwise chemogenomic screening approach is an efficient strategy to exploit drug poly-pharmacology for the identification of core vulnerabilities, that could be further therapeutically exploited.

Targeting core vulnerabilities uncovers synergistic drug combinations in GBM

In order to therapeutically exploit the core vulnerabilities identified by our chemogenomic screens, we established a biology-guided drug combination screen using available inhibitors of 6 core vulnerabilities: AURKA inhibitor Alisertib, CDK1 inhibitor Dinaciclib, HDAC3 inhibitor Panobinostat, CHEK1 inhibitor Prexasertib, PLK1 inhibitor Rigosertib and mTOR inhibitor Vistusertib (Figure S2a). These inhibitors were screened in the murine GL261 GBM cell line in combination with a custom-made library of 88 FDA-approved compounds, of which 15 repurposed drugs identified as pharmacological hits in our drug screening (Fig. 1a and b) together with 15 epidrugs, 49 targeted therapies and 9 additional repurposed drugs. These agents were chosen because they were either approved by the US Federal Drug Administration (FDA) or in advanced clinical development and were considered potentially useful in treating brain cancer patients based on prior clinical and preclinical evidence (Table S1). We used the difference in AUC between the combinatorial treatment and the monotherapy condition. Combinations with differences in AUC of more than 5%.mol.L^{-1} were considered as potentially synergistics and below −5%.mol.L^{-1} as potentially antagonistics. A full report of this combination screen can be found in Table S8. Amongst the 528 tested pair-wise combinations, 4.9% appeared to have a potential synergistic effect (Figure S2b–g). Since combinations with Alisertib, Prexasertib, Panobinostat and Vistusertib were the most favorable (4.5, 5.7, 5.7 and 10.2% of potential synergisms, respectively), we focused our analyses on combinations involving these 4 inhibitors (Figure S2d–g). Amongst the 88 tested drugs, 15 were epidrugs including 7 BET inhibitors, 4 HDAC inhibitors and 4 other epidrugs (Fig. 3a). Our results indicated that the combination of Alisertib or Vistusertib with most of the BET inhibitors was potentially synergistic, while it was mostly antagonistic when combined with Panobinostat, and to a lesser extent with Prexasertib (Fig. 3a). These results were reflected by a decrease in the IC_{50} of BET inhibitors when co-administered with Alisertib and Vistusertib and, in contrast, an increase in the IC_{50} of these drugs when co-administered with Prexasertib and Panobinostat (Figure S3a). Regarding the 24 repurposed drug tested in our library, 2 potentially synergistic combinations were observed between Vistusertib/Aripiprazole and Panobinostat/Quinacrine, which was illustrated by a decrease in the IC_{50} of both repurposed drugs when combined with a mTOR or HDAC3 inhibitor (Fig. 3b and Figure S3b). Finally, 49 targeted therapies were tested covering major signaling pathways involved in cancer (Fig. 3c). Our combination drug screen highlighted a potential synergism between MEK inhibitors and Alisertib or Prexasertib, while a potential antagonism was observed with Panobinostat and to a lesser extent with Vistusertib (Fig. 3c). This was also demonstrated by the decrease in IC_{50} values of both MEK inhibitors, Mirdametinib and Selumetinib, when combined with Alisertib or Prexasertib and their increase when associated with Panobinostat or Vistusertib (Figure S3c).

To confirm the interactions underlined by our biology-driven drug combination screen, we assessed them using the human U87 and murine GL261 GBM cell lines in 3D spheroid culture conditions treated during 15 days. We focused our validation experiments on two potentially synergistic drug combinations: Alisertib/Birabresib (Fig. 3a and Figure S3a), Prexasertib/Mirdametinib (Fig. 3c and Figure S3c) and one potentially antagonistic combination Panobinostat/Birabresib (Fig. 3a and Figure S3a). A 6 × 5 matrix that contained the two compounds at different concentration ratios was

revealed for the 83 hit compounds. Amongst them, 292 were targeted by at least 3 hit compounds and selected to build a focused siRNA library. The T98G, U87 and its derivative U87vIII GBM cell lines were individually transfected with 3 siRNA sequences (5 nM) for each of the 292 targets/interactors (n = 3 per condition from one experiment, followed by validation run). Cell viability was assessed by high-content imaging following Hoechst 33342 staining. Polar plot of 22 gene hits, which their gene expression downregulation decreased the cell viability in each tested cell line by at least 20%. Polar plot was made up of 10 data rings, each radial point representing a ten percent increment of the cell viability on a scale from 0 (inner radial point) to 100 (outer radial point). (**d**) Heat map representing the gene effect score of the 22 gene hits in 3 GBM cell lines, extracted from the CRISPR screen cohort data from the online Dependency Map portal. Right panel shows the protein–protein interaction network of the 9 hits identified as core vulnerabilities in all tested GBM cell lines (Gene effect score <−0.5; https://string-db.org/).

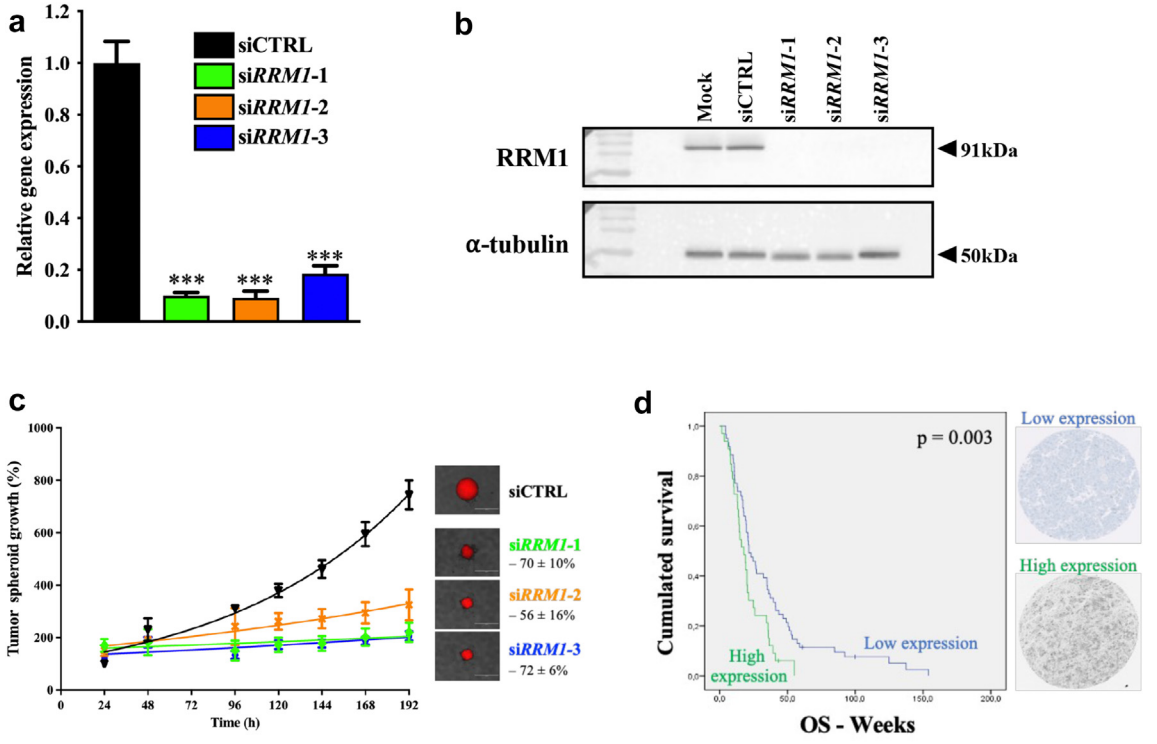

Fig. 2: **Functional validation of top gene hit *RRM1* in glioblastoma cells and patient samples.** (**a**) *RRM1* relative gene expression following 48 h transfection of U87 cells with negative control siRNA and 3 different siRNA sequences targeting *RRM1*, as evaluated by qRT-PCR using *YWHAZ* as housekeeping gene. All the values are the average of four independent experiments ± standard error of mean (S.E.M), with a technical triplicate in each experiment; ***, $p < 0.001$ (Student's t-test). (**b**) Representative Western blot showing RRM1 protein expression following 72 h siRNA transfection, using α-tubulin as loading control. (**c**) The mtDsRed-expressing U87 tumor spheroid growth following siRNA transfection assessed by daily fluorescence measurements. All the values are the average of four independent experiments ± standard error of mean (S.E.M), with a technical triplicate in each experiment; *, $p < 0.05$; **, $p < 0.01$; ***, $p < 0.001$ (Student's t-test). Representative photographs of tumor spheroids at day 8 and mean decrease in spheroid growth ± S.D are included in insert (*right*). *Scale bar*, 1 mm. (**d**) Kaplan–Meier survival estimate of GBM patients (n = 97) according to RRM1 protein expression assessed by immunohistochemistry. Cox proportional hazards regression *p* value is shown and representative pictures of tumor samples displaying low (*top*) and high (*bottom*) RRM1 expression are included (*right*).

created, allowing to cover a large range of drug combinations. To assess the synergy of the two compound treatments, the Bliss score was calculated using the SynergyFinder web application (https://synergyfinder.fimm.fi).[20] As expected by our screen results, we found an antagonistic interaction between Birabresib and Panobinostat in GL261 cells, as demonstrated by a Bliss score of –2.0 ± 4.0 (Fig. 4a and d). In sharp contrast, a synergistic effect was shown in the U87 spheroid model with a Bliss score of 8.5 ± 4.3 (Fig. 4g and j). Indeed, a decrease in the U87 spheroid viability was observed with monotherapies of 25 nM Panobinostat and 1 μM Birabresib (52.5 ± 9.3% and 22.9 ± 17.7% respectively, Fig. 4g and j), that was even more important following combination treatment (87.3 ± 7.1% in comparison to untreated cells; Fig. 4j).

Our validation assay also demonstrated that the combination of CHK1 inhibitor Prexasertib and MEK inhibitor Mirdametinib produced a synergistic effect in both 3D spheroid models (Fig. 4b, e, h and k) with an overall Bliss score of 7.9 ± 3.7 in GL261 and 2.9 ± 2.9 in U87 (Fig. 4b and h). We also found that the combination of AURKA inhibitor Alisertib and BET inhibitor Birabresib produced a highly synergistic effect with an overall Bliss score of 14.9 ± 1.9 in GL261 and 6.5 ± 0.7 in U87 (Fig. 4c and i). Indeed, while a small drop in GL261 spheroid viability was observed with monotherapies of 25 nM Alisertib and 100 nM Birabresib (16.2 ± 4.1% and 2.7 ± 3.7% respectively, Fig. 4f), the synergistic score of their combination was reflected by a decrease of 56.6 ± 3.4% in comparison to untreated cells (Fig. 4f). Similar results were obtained with the U87 GBM cell line, in which the association of 25 nM Alisertib and 1 μM Birabresib resulted in a decrease in tumor spheroid viability of 59.2 ± 12.5% after 15 days in comparison to control, while each monotherapy reduced

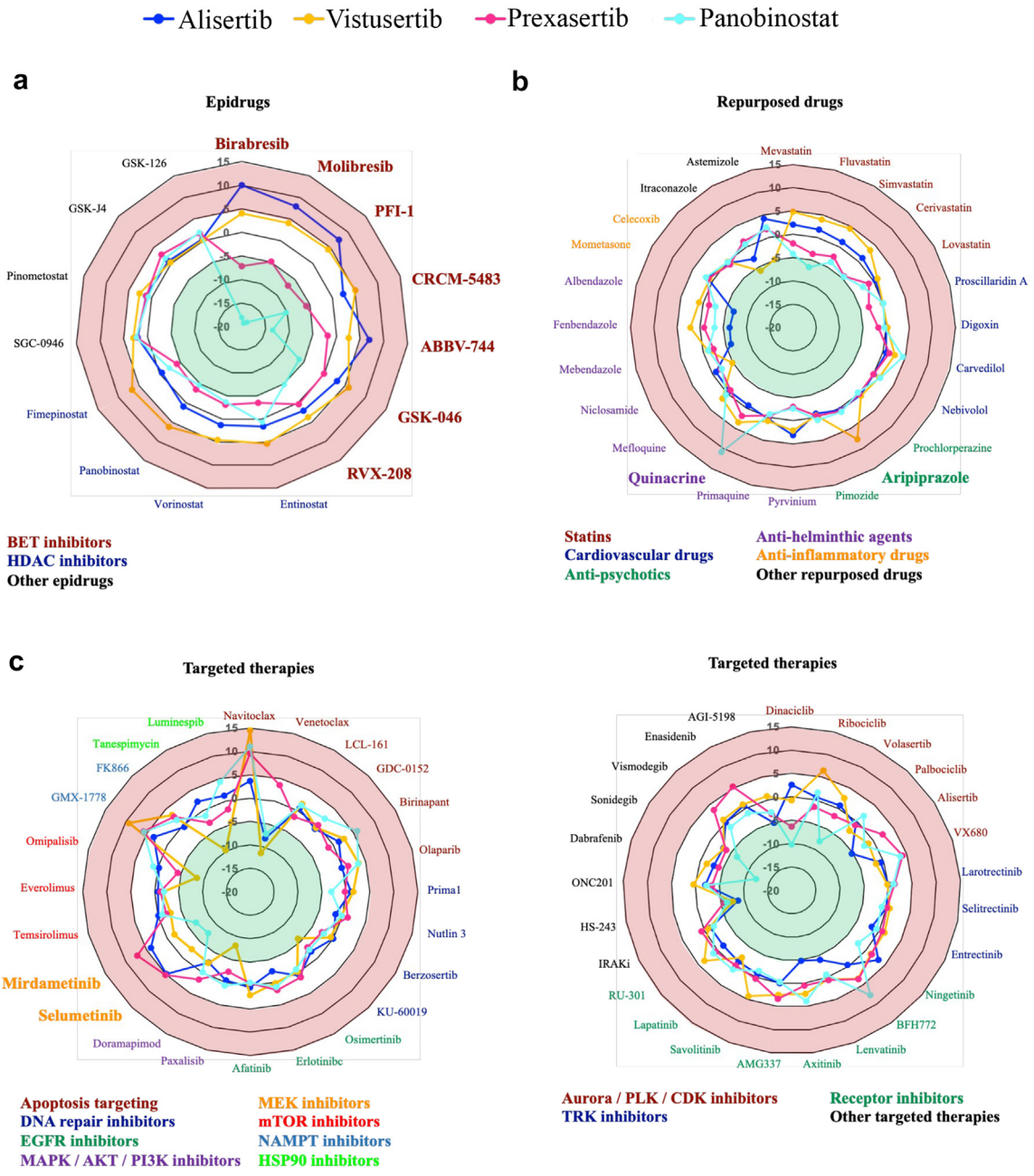

Fig. 3: **A biology-guided drug combination screen reveals potential synergistic treatments in GBM.** A custom-made library containing 88 drugs was screened on the murine GL261 GBM cell line in a dose-effect manner alone or in association with Alisertib 1 µM, Vistusertib 250 nM, Prexasertib 10 nM or Panobinostat 10 nM (technical duplicate per condition in one experiment). After 72 h of drug incubation, cell viability was assessed using CellTiter Glo®. Radar plots show the difference in AUC between the combinatorial treatment and the monotherapy condition (combination with Alisertib: dark blue line, Vistusertib: yellow line, Prexasertib: pink line and Panobinostat: light blue line). Radar plots were made up of 7 data rings on a scale from −20%.mol.L^{-1} (inner ring) to +15%.mol.L^{-1} (outer ring) with an increment of 5%.mol.L^{-1}. Green rings represent potentially antagonistic combinations (AUC differences <−5%.mol.L^{-1}) and the red ones indicate potentially synergistic treatments (AUC differences >5%.mol.L^{-1}). Radar plots representation of data obtained with (**a**) 15 epidrugs, (**b**) 24 repurposed drugs, and (**c**) 49 targeted therapies.

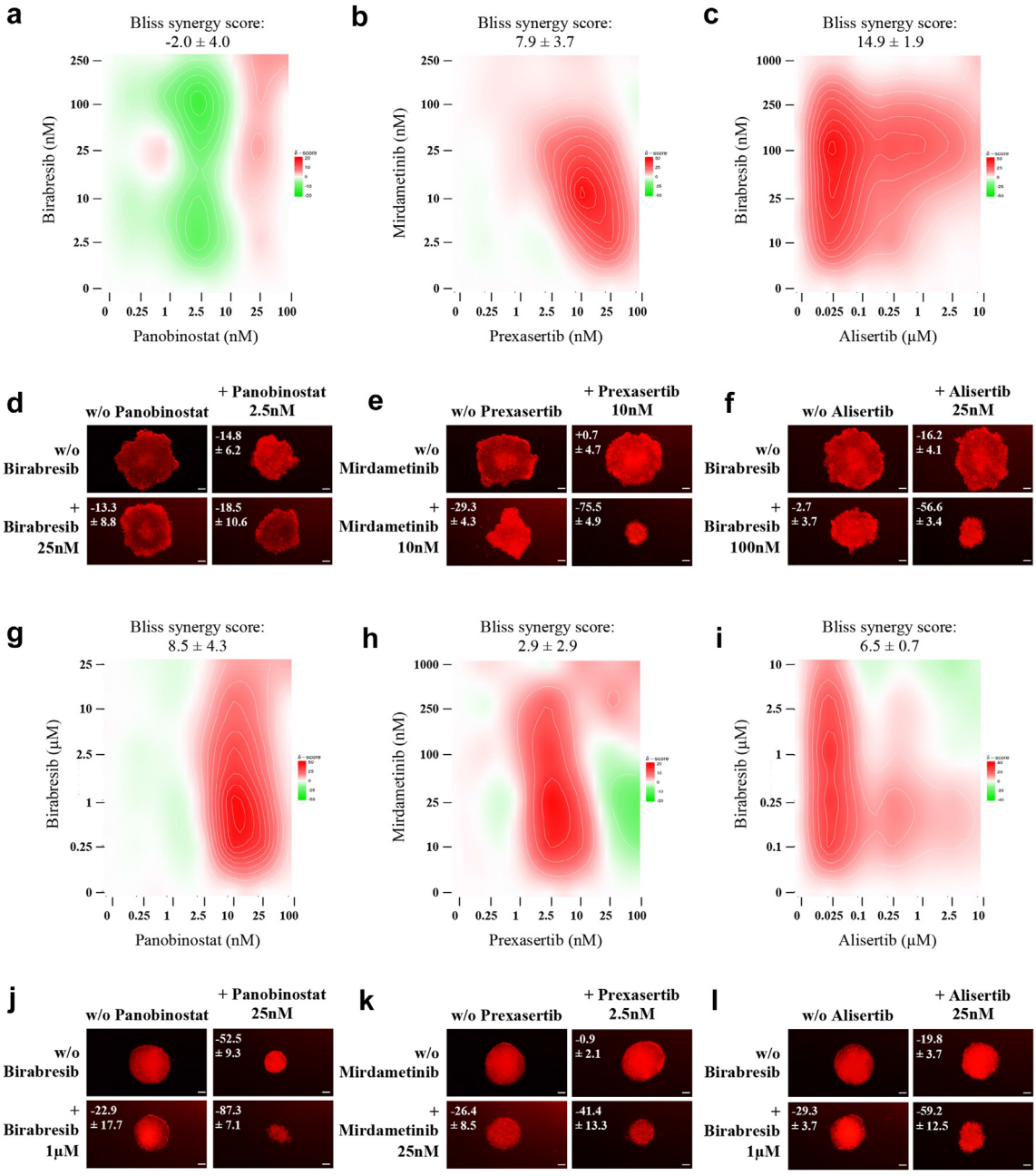

Fig. 4: **Validation of drug combinations in spheroid GBM models.** A 6 × 5 matrix was used to test drug combinations in GL261 (panels **a** to **f**) and U87 (panels **g** to **l**) spheroid models. Heat maps representing the Bliss score for three tested combinations: Panobinostat/Birabresib (panels **a** and **g**), Prexasertib/Mirdametinib (panels **b** and **h**) and Alisertib/Birabresib (panels **c** and **i**). Representative photographs of GL261 (panels **d** to **f**) and U87 (panels **j** to **l**) tumor spheroids at day 14 and mean decrease in spheroid growth are indicated. *Scale bar,* 1 mm. All values are the average of at least three independent experiments ± standard error of mean (S.D), with a technical duplicate in each experiment.

the spheroid viability of 19.8 ± 3.7% and 29.3 ± 3.7%, respectively (Fig. 4l). In order to ascertain the potent synergism identified between Alisertib and Birabresib, we used two different patient-derived glioblastoma-initiating cell lines: the mesenchymal GBM6 and proneural GBM9 models, previously generated and characterized in our lab.[12,13] Our results confirmed a synergistic effect with an overall Bliss score of 8.5 ± 1.2 in GBM6 and 12.9 ± 1.5 in GBM9 tumor spheroids (Figure S4a and b). Moreover, to reinforce the relevance

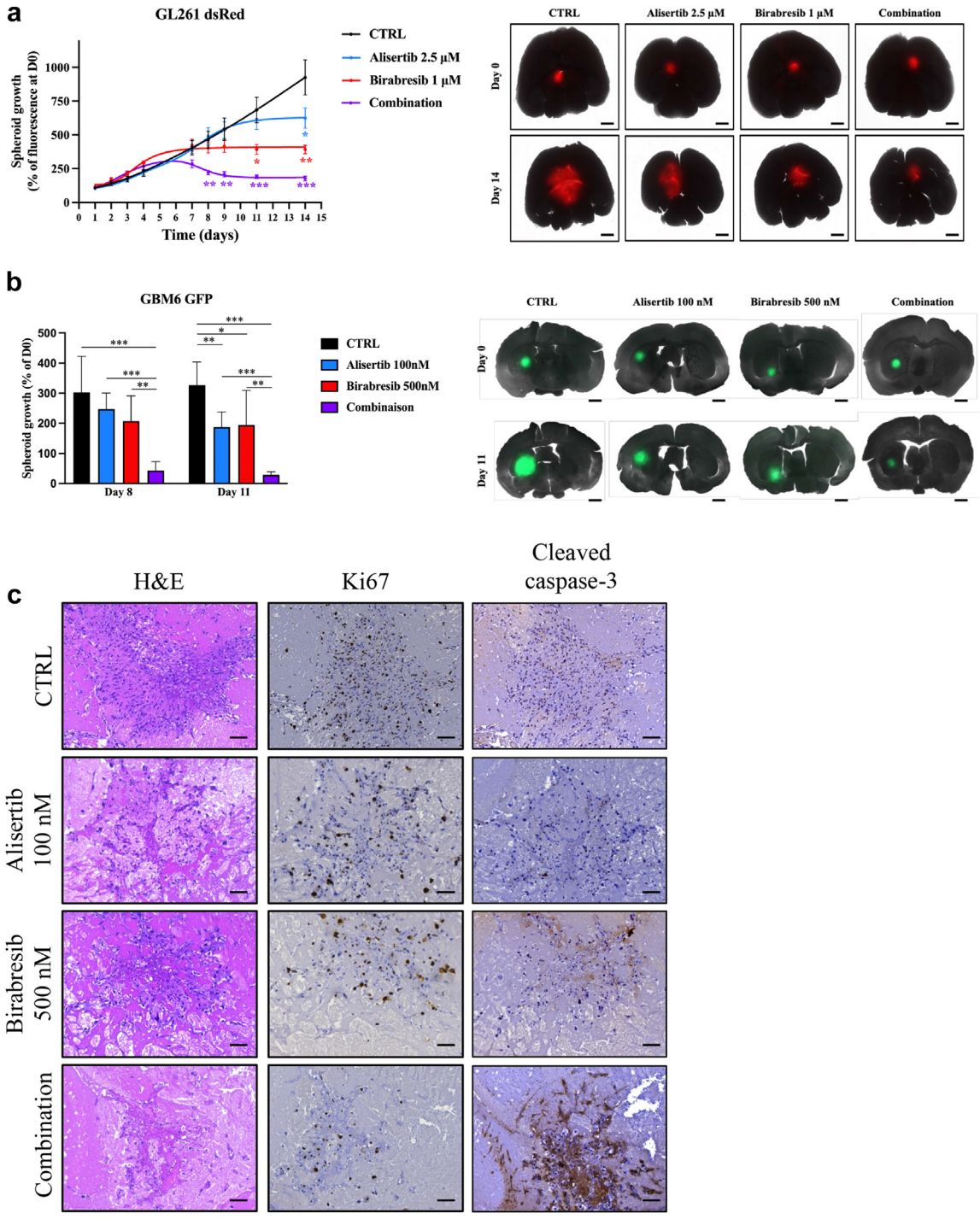

***Fig. 5:* Alisertib/Birabresib combination is highly effective in *ex vivo* GBM organotypic model.** (**a**) For 5 consecutive days, mouse brain slices with mtDsRed-expressing GL261 were exposed to daily doses of Alisertib 2.5 µM alone (blue), Birabresib 1 µM alone (red) or their combination (purple). GL261 tumor growth was measured over 14 days by acquisition of the mtDsRed signal with the Pherastar® plate reader (well-scanning mode). Values are the average of n = 5 samples per condition, *Error bars*, S.D; *, $p < 0.05$; **, $p < 0.01$; ***, $p < 0.001$, ANOVA test. Representative photographs, acquired with the JuLi™ Stage live imaging system, of mtDsRed-expressing GL261 tumor micro-masses grafted in slices of healthy mouse brain. *Scale bar:* 1 mm. (**b**) For 5 consecutive days, mouse brain slices grafted with GFP-expressing GBM6 cells were exposed to daily doses of Alisertib 100 nM alone, Birabresib 500 nM alone or their combination. Quantification of GFP-GBM6 tumor size measured over 11 days using ZEISS ZEN software. Results were expressed as percentage of spheroid growth in treated vs. control organotypic models (CTRL at day

of this combination strategy, we tested the selective AURKA inhibitor LY3295668 in combination with Birabresib and another BET inhibitor Molibresib in combination with Alisertib in the GL261 cell line. We found that both drug combinations resulted in a light synergistic effect with overall Bliss scores of 4.4 ± 1.2 and 6.1 ± 0.8 for LY3295668/Birabresib and Alisertib/Molibresib, respectively (Figure S4c and d). These results were reflected by a decrease in tumor spheroid viability of 75.1 ± 0.6% after 15 days of treatment with the combination of LY3295668/Birabresib at 250 nM in comparison to control, while monotherapies reduced spheroid viability by 31.5 ± 0.8% and 50 ± 0.5% for LY3295668 and Birabresib, respectively (Figure S4e). Similar results were obtained with Alisertib and Molibresib at 250 and 500 nM, respectively (Figure S4f). Finally, to evaluate the clinical relevance of the canonical targets of Alisertib and Birabresib, we used freely available datasets in the R2 platform to compare gene expression in GBM subtypes and normal brain tissue. Transcriptomic analysis showed that *BRD2, BRD3, BRD4* and *AURKA* expression levels are significantly up-regulated in GBM tumors of all subtypes as compared to normal brain tissue ($p < 0.01$; Figure S4g, ANOVA test). Collectively, our results underlined that our approach to rationally design drug combination screening represents a valuable strategy to rapidly discover pharmacological synergisms.

Dual BET/AURKA inhibition is highly synergistic in GBM models *ex vivo* and *in vivo*

Our data indicated that Alisertib, a selective inhibitor of core GBM vulnerability Aurora kinase A, was highly synergistic with Birabresib, a pan-BET inhibitor in all tested *in vitro* GBM cell models (Fig. 4c, f, i and l and Figure S4a and b). To further evaluate the potential of dual AURKA/BET inhibition in more clinically-relevant conditions, we developed an organotypic *ex vivo* model in which murine GL261 GBM spheroids stably expressing mtDsRed were grafted into slices of healthy mouse brain. These innovative cultures were exposed to 2.5 µM of Alisertib, 1 µM of Birabresib or their combination during 5 consecutive days. After 8 days, our data showed that both monotherapies have no significant impact on the growth of GL261 tumor masses (+11 ± 6 and −13 ± 3%, respectively; Fig. 5a, ANOVA test), while the combinatorial treatment resulted in a significant reduction of 53 ± 2% in comparison to control ($p < 0.01$; ANOVA test, Fig. 5a). After 14 days, Alisertib led to a significant decrease in tumor spheroid growth (−36 ± 4% in comparison to control; $p < 0.05$, ANOVA test) and so did Birabresib (−58 ± 3% in comparison to control; $p < 0.01$, ANOVA test) (Fig. 5a). The synergistic effect of Alisertib/Birabresib was even exacerbated over time, with the combination decreasing tumor growth by 81 ± 2, 70 ± 2 and 55 ± 2% in comparison to control, Alisertib alone and Birabresib alone, respectively ($p < 0.001$; ANOVA test, Fig. 5a). To further strengthen our results, we developed a second organotypic *ex vivo* model using patient-derived GBM-initiating cells GBM6 stably expressing GFP (Fig. 5b). Eight days post-engraftment, both monotherapies had no significant impact on the growth of GBM6 tumor masses (−18 ± 5 and −31 ± 8%, for 100 nM Alisertib and 500 nM Birabresib, respectively; $p > 0.05$, ANOVA test, Fig. 5b), while the combinatorial treatment resulted in a significant reduction of 86 ± 3% in comparison to control ($p < 0.001$; ANOVA test, Fig. 5b). The observed effect of the drug combination was even more pronounced over time, with the combination leading to a decrease in tumor masses of 91 ± 2% in comparison to control after 11 days ($p < 0.001$; ANOVA test, Fig. 5b). Finally, Ki-67 and cleaved caspase-3 immunohistochemistry performed on tumor slices at day 11 showed a decrease in tumor cell proliferation associated with a strong increase in tumor cell death as a result of the combinatorial treatment (Fig. 5c).

To validate the synergism between Alisertib and Birabresib against GBM *in vivo*, we finally used an orthotopic syngenic mouse model where murine GL261 GBM cells were transplanted by stereotaxy into the corpus callosum of immunocompetent C57BL/6 mice. One week later, mice were randomized and treated *p.o.* with either vehicle alone (1/10 DMSO in corn oil), Alisertib alone (25 mg/kg), Birabresib alone (75 mg/kg) or the combination of both drugs. Monotherapies only marginally extended the median survival from 25.5 days observed for the vehicle control mice to 28 days for Alisertib alone and 30.5 days for Birabresib alone (Fig. 6a and Table 1). In contrast, the combination treatment increased the median survival of GL261-bearing mice to 48 days ($p = 0.0002$, 0.0031 and 0.0131 in comparison to vehicle, Alisertib alone and Birabresib alone, respectively; log rank test, Fig. 6a and Table 1). The combination thus increased the therapeutic benefit of Alisertib and Birabresib alone by 9- and 4.5-fold, respectively (Table 1). It is worth to note that 2 animals treated with the combination were alive and well at study completion (t = 120 days). Moreover, the survival study showed that treatment with Alisertib or Birabresib alone or in combination was well-tolerated and did not result in increased toxicity, as evidenced

0). Values are the average of n = 6 samples per condition, *Error bars*, S.D; *, $p < 0.05$; **, $p < 0.01$, ***, $p < 0.001$, ANOVA test. Representative images of GFP-GBM6 tumor spheroids grafted in slices of healthy mouse brain. Scale bars: 1 mm. (**c**) Representative images of hematoxylin–eosin (H&E), Ki67 and cleaved caspase-3 staining of GBM6-GFP tumours from organotypic co-cultures treated with vehicle alone (CTRL), Alisertib 100 nM alone, Birabresib 500 nM alone or their combination at day 11. Scale bar: 100 µm.

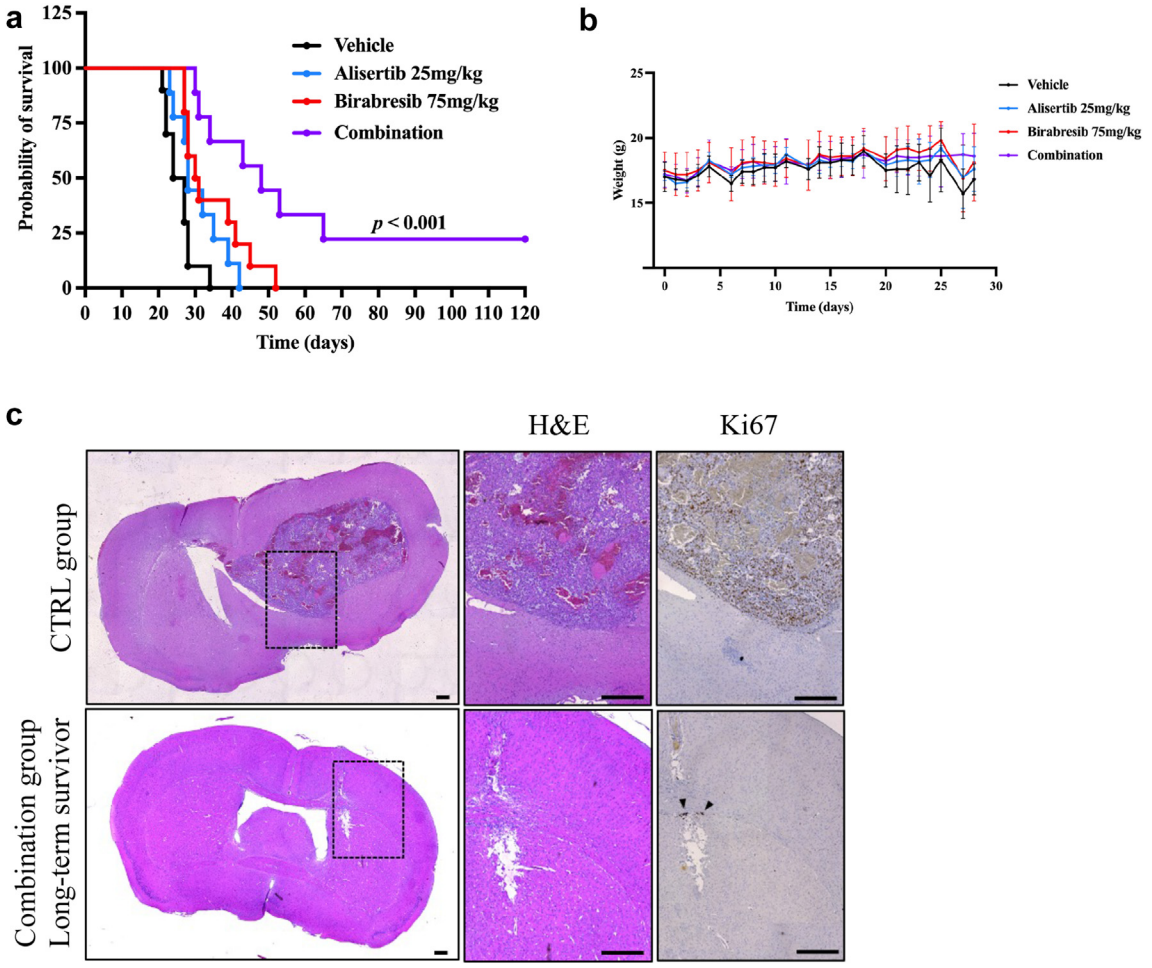

***Fig. 6:* Alisertib/Birabresib combination is highly effective in *in vivo* orthotopic mouse model.** (**a**) Kaplan–Meier survival and (**b**) weight of murine GBM-bearing mice treated by oral gavage 5 time a week over 3 weeks, starting 1 week after orthotopic injection of GL261 cells, with vehicle only (1/10 DMSO in corn oil; vehicle; *black*), Alisertib (75 mg/kg; *blue*), Birabresib (25 mg/kg; *red*) or the combination of both drugs (*purple*). ***, $p < 0.001$, log rank test (Mantel–Cox test). (n >9 mice per group) (**c**) Representative images of hematoxylin–eosin (H&E) and Ki67 staining of GL261 tumors from mice treated with vehicle (CTRL group at day 24; top panel) or combination of Alisertib and Birabresib (at day 120; bottom panel). Arrowheads show Ki67 positive cells. Full brain coronal section (top and bottom left panels) and magnification (top and bottom middle and right panels). Scale bar: 500 µm.

by a lack of significant change in animal weight during the treatment (Fig. 6b). Anatomopathological examination revealed a massive tumor mass invading brain parenchyma with high proliferation index in control mice euthanized at day 24 (Fig. 6c, top right panel). Conversely, one of the long-term survivors displayed no evidence of disease at day 120 while the other had a very small tumor with rare proliferating cells, according to

Treatment (mice per cohort)	Median survival (days)	Log-rank test (vs. vehicle)	Log-rank test (vs. Alisertib)	Log-rank test (vs. Birabresib)
Vehicle (n = 10)	25.5	N/A	0.0409 *	0.0045 **
Alisertib (n = 9) 25 mg/kg per os, 5 days per week	28	0.0409 *	N/A	0.2545
Birabresib (n = 10) 75 mg/kg per os, 5 days per week	30.5	0.0045 **	0.2545	N/A
Alisertib + Birabresib (n = 9)	48	0.0002 ***	0.0031 **	0.0131 *

***Table 1:* Median survival of mice harboring GL261 orthotopic xenograft tumors.**

Ki-67 immunohistochemistry (Fig. 6c, bottom right panel). In conclusion, our results indicate that dual inhibition of BET proteins and Aurora kinase A is highly synergistic and could be used as an alternative therapeutic strategy in GBM.

Discussion

Despite significant advances in the understanding of GBM biology in recent years, no major breakthrough has been translated into the clinic yet and the standard-of-care has been solely based on radiotherapy with Temozolomide for more than 15 years.[8] In this study, we developed a data-driven approach in order to reveal core vulnerabilities and highlight potential synergistic drug combinations for this unmet medical need.

The predominant paradigm in drug discovery has been the search for maximally selective drugs that act on individual targets. The limitations of this approach are perfectly illustrated by the discovery of EGFR mutations in ~40% of GBM patients,[22] yet EGFR targeted therapies failing in clinical trials due to inefficient drug penetration and distribution in the brain as well as the very high inter- and intra-tumor heterogeneity of GBM.[23] In this context, combination therapy is the most efficient strategy since the association of two drugs can be synergistic and thus allow better anti-tumor response with lower concentration of single agents. Nevertheless, with more than 5000 approved-drugs or compounds in clinical development, pinpointing synergistic drug combinations represents a major challenge. Herein, we aimed at streamlining the identification of potent combinations by exploiting drug poly-pharmacology using commercially available libraries of compounds with known targets. We hypothesized that the annotated targets of a pharmacological hit may be involved in modulating GBM cell survival, and could thus represent targetable vulnerabilities. We developed a pipeline for the deconvolution of readily druggable targets directly from a high-throughput screening based on drug repurposing principle, followed by a focused siRNA library screen to prioritize targets. As a result, we identified nine core vulnerabilities in GBM: *RRM1*, *PLK1*, *CHEK1*, *AURKB*, *CDK1*, *AURKA*, *FRAP1*, *HDAC3* and *ATP1A1*. Large pharmacological screens are rarely followed by target validation studies, which prevent the discovery of potential biomarkers. Here to ascertain our method, we focused our functional validation experiments on the top gene hit of our chemogenomic screen approach *RRM1*. Ribonucleotide reductase is the key enzyme that catalyzes the production of deoxyribonucleotides for DNA replication.[21] Several studies have shown that *RRM1* could act as a tumor suppressor gene in lung and pancreas carcinomas.[24–26] These effects have been notably linked to the induction of PTEN expression and an increase in DNA damage repair.[27,28] Moreover, RRM1 is also the predominant cellular determinant of the efficacy of the nucleoside analogue drug gemcitabine. Indeed, studies have reported that high RRM1 expression was associated with a poor prognosis in patients treated with gemcitabine for their non-small cell lung, pancreatic, biliary or bladder cancers.[29–32] Herein, we provide strong evidence supporting an oncogenic role of *RRM1* in GBM. Our results are consistent with recent data demonstrating that high RRM1 expression leads to GBM growth and poor patient outcome.[33,34] Moreover, RRM1 is highly expressed in brain metastasis and associated with Temozolomide resistance.[35,36] In this study, our results highlight the prognostic role of RRM1 in GBM and advocate for the rapid development of potent RRM1 inhibitors with good brain penetration since current RRM1 inhibitors, including gemcitabine and clofarabine, cannot cross the blood brain barrier. Further studies focusing on associated targets regulating RRM1 oncogenic role in GBM are necessary to fully decipher its functions and explain the observed discrepancy of RRM1 functions between different cancer types.

Multiple high-throughput screening campaigns have been performed to discover new therapeutic options in cancer. The emergence of the CRISPR-Cas9 technology has enabled genome-wide screens, which allow the identification of core vulnerabilities governing cell survival across all cell types, including in GBM.[37–39] However, these functional studies have rarely been combined with pharmacological screens to therapeutically exploit the identified vulnerabilities. Moreover, to reach effective and sustained clinical responses, drug combinations that simultaneously inhibit multiple pathways in cancer cells are needed. Most studies in the field usually focus on combination screens involving conventional chemotherapy agents with large non-specific small molecule libraries. Herein, we attempted to therapeutically leveraged the results of our chemogenomic data by designing a biology-driven drug combination screen. We built a focused drug library with compounds chosen based on the following criteria: *i)* approved by the US FDA or in advanced clinical development, *ii)* considered potentially useful in treating brain tumors based on prior clinical and preclinical evidence, and *iii)* able to cross the blood–brain barrier. Using the biological and functional information obtained from our dual drug and siRNA screen, six out of the nine core vulnerabilities identified in GBM were targeted to perform a combination drug screen and quickly reveal potentially synergistic drug combinations. Our results indicated that synergism is rare with only 4.9% of the 528 tested pair-wise combinations described as potentially synergistic, in line with recent large-scale studies.[40,41]

The MAPK pathway being one of the most commonly mutated oncogenic pathways in cancer, the

therapeutic landscape of antitumor agents targeting this pathway has rapidly expanded, including several MEK inhibitors.[42] While studies have demonstrated the potential of MEK inhibitors in association with inhibitors of the PI3K/mTOR pathway,[43,44] our drug combination screen with mTOR inhibitor Vistusertib indicated no potential synergy with the two tested MEK inhibitors Mirdametinib and Selumetinib. However, our results highlighted the potential synergistic interaction of CHK1 inhibitor Prexasertib with MEK inhibitors. Owing to its role in therapeutic resistance and oncogenesis, selective inhibitors of the cell cycle checkpoint kinase CHK1 are currently under pre-clinical and clinical investigations.[45] CHK1 has been shown to play a role in cell proliferation, radioresistance and Temozolomide-induced senescence in GBM.[46,47] Moreover, few studies showed that targeting the MEK pathway potentiates CHK1 inhibitor in multiple myeloma models, primary human glioma cells and a neuroblastoma cell line.[48–50] In line with these studies, using two GBM 3D spheroid models, we demonstrated the synergistic potential of combining Prexasertib with Mirdametinib, which warrants further investigation to confirm its therapeutic potential and clinical relevance in GBM.

Accumulating evidence demonstrates that aberrant epigenetic regulation of gene function plays a major role in carcinogenesis and tumor escape from therapy.[51] This has led to an increase in epigenetic drugs or epidrugs in development, including BET inhibitors (BETi).[52,53] Owing to the interplay among various epigenetic processes, combining several epidrugs has emerged as a promising approach to anticancer therapy. Recent studies have provided mechanistic and pre-clinical evidence for the combination of HDAC inhibitors (HDACi) with BETi, even leading to the development of dual inhibitors.[54–57] Herein, our combination drug screen revealed that HDACi Panobinostat mostly antagonizes with all tested BETi in the murine GL261 cell line. While these unexpected results were confirmed in the GL261 spheroid model using Panobinostat and Birabresib, a synergistic effect was observed with the same drug combination in the U87 spheroid model. A recent study also indicated that HDACi combined with BETi was synergistic in two human GBM-sphere lines.[58] Our results thus suggest a cellular context dependance and warrant further molecular investigations to fully decipher the mechanism of action of the dual HDAC/BET inhibition by identifying their molecular targets.

Using different small-molecule inhibitors, our results also highlighted the therapeutic potential of dual BET and AURKA inhibition in 4 different GBM cell lines, including two patient-derived glioblastoma-initiating cell models harboring specific GBM molecular characteristics.[12,13] The therapeutic potential of this combination has been previously shown in neuroblastoma models.[59,60] The synergistic effect has been notably linked to the inhibition of MYCN expression, as also demonstrated in an *in vitro* GBM study.[61] Moreover, by developing an integrative drug and disease signature approach, Stathias et al. recently identified JQ1 and Alisertib as a synergistic combination in GBM, which was validated in a subcutaneous model of GBM.[62] Nevertheless, as the high rate of attrition in cancer drug development is partly due to a lack of predictive preclinical models,[63,64] findings need to be carefully evaluated using a range of model systems. Herein, to confirm our results obtained with dual BET/AURKA inhibition on 3D spheroid GBM models and its therapeutic potential, we developed two organotypic brain models in which GBM tumor progression was followed over time, using the murine GL261 cell line and a human primary GBM-initiating cell model. These *ex vivo* tissue cultures are described as highly relevant models to study the evolution of pathologies and to test their response to different therapeutic strategies, including in brain diseases.[65] This co-culture system can keep brain tissues alive in incubation chambers mimicking natural conditions. Our results showed that the synergistic effect of Alisertib/Birabresib was maintained in both models and even exacerbated over time. To increase the complexity of our pre-clinical model and strengthen our results, we finally used an orthotopic syngenic mouse model. We showed that the orally administered drug combination significantly increased the median survival of GBM-bearing immunocompetent mice, without any observed side effects. Moreover, our transcriptomic analysis showed that *AURKA* and *BRD2/3/4* gene expressions are up-regulated in GBM tissues in comparison to healthy brain tissues, reinforcing the rationale of dual BET and AURKA inhibition in GBM. Since Alisertib has been safely evaluated in a phase I trial for recurrent high-grade glioma patients[66] and several clinical trials have been undertaken or are ongoing with both drugs separately in GBM patients [NCT02186509, NCT02296476], our preclinical data strongly support the therapeutic relevance of the Birabresib/Alisertib combination in GBM.

This study points out that dual inhibition of AURKA and BET represents a potential therapeutic avenue in GBM, and provides a strong foundation for future clinical trials. Our findings also highlight the prognostic value of RRM1 in GBM, supporting the interest to develop RRM1 inhibitors for GBM therapies. Moreover, our data demonstrate the feasibility and efficiency of our approach to identify disease-relevant targets by harnessing drug poly-pharmacology and using target deconvolution, and to therapeutically leverage these vulnerabilities by designing biology-guided drug combinations. This strategy could potentially be applied to any refractory cancers, thus opening major therapeutic avenues.

Contributors

Conceptualization: E.P and M.L.G. Formal analysis: E.P, M.L.G, J.A.B, R.B, M.P.M, G.P, P.M, N.B.K, C.C and D.F.B. Investigation: E.P, M.L.G, J.A.B, R.B, M.P.M, B.M, K.M, G.P, T.W.F, G.M.A, N.B.K, P.M,

C.C and D.F.B. Funding acquisition: M.L.G and E.P. Methodology: E.P, M.L.G, J.A.B, P.P, K.M, G.P, T.W.F, G.M.A, P.M, O.C, D.B and D.F.B. Project administration: E.P, M.L.G, D.F.B and E.T. Supervision: E.P and M.L.G. Validation: E.P, M.L.G, J.A.B, D.F.B, E.T, O.C, D.B, M.C, N.A and X.M. Visualization: E.P, M.L.G, J.A.B, R.B, M.P.M, N.B.K and C.C. Writing—original draft: J.A.B, E.P and M.L.G. Writing, review & editing: E.P, M.L.G, J.A.B, R.B, G.P, N.B.K, C.C, X.M, N.A, M.C, E.T and D.F.B. All authors have read and approved the final manuscript.

Data sharing statement

Raw data of the high-throughput drug screening and drug combination screening are available in the supplementary table files. The other data and materials are available from the corresponding authors upon reasonable request.

Declaration of interests

The authors have declared no conflict of interest.

Acknowledgements

We thank the 'HiTS' platform (Carine Derviaux; https://www.crcm-marseille.fr/equipes/plateformestechnologiques/hits-ipcdd/) for the help with the combination drug screening. The authors would like to thank the AP-HM Tumor Bank (authorization number: AC2018-31053; CRB BB-0033-00097) for providing GBM tissue samples, and the ARTC-Sud patients association (*Association pour le Recherche sur les Tumeurs Cérébrales*).

This work was exclusively funded by institutional grants and donations from non-for-profit organizations, which had no influence on the direction of this research. It included research grants attributed to EP: Marie Sklodowska-Curie Fellowship from the European Research Council (FP7-PEOPLE-2013-IIF #626794), "Pépiniere d'Excellence" grant from the AMIDEX of Aix Marseille University (funded by socio-economic partners) or "Pépiniere d'Excellence" grant from the Aix Marseille University (funded by socio-economic partners), Translational Research grant from the French National Cancer Institute (PRT-K19-135, INCa), and research grants from Eva pour la Vie and Wonder Augustine, and to MLG: post-doctoral fellowship from the ARC Foundation ($\#_{ARCPDF22020070002553}$). This work was also supported by the SIRIC Marseille (Integrated Oncology Research Site, INCa), the Canceropole PACA and several not-for-profit organisations (Association Léa, Association Cassandra, Le sourire de Lucie, Vocaliz' et Nos p'tites Etoiles).

Appendix A. Supplementary data

Supplementary data related to this article can be found at https://doi.org/10.1016/j.ebiom.2023.104752.

References

1 Kumar-Sinha C, Chinnaiyan AM. Precision oncology in the age of integrative genomics. *Nat Biotechnol*. 2018;36(1):46–60.
2 Xiang Y, Ye Y, Zhang Z, Han L. Maximizing the utility of cancer transcriptomic data. *Trends Cancer*. 2018;4(12):823–837.
3 Hopkins AL. Network pharmacology: the next paradigm in drug discovery. *Nat Chem Biol*. 2008;4(11):682–690.
4 Al-Lazikani B, Banerji U, Workman P. Combinatorial drug therapy for cancer in the post-genomic era. *Nat Biotechnol*. 2012;30(7):679–692.
5 Peters JU. Polypharmacology - foe or friend? *J Med Chem*. 2013;56(22):8955–8971.
6 Anighoro A, Bajorath J, Rastelli G. Polypharmacology: challenges and opportunities in drug discovery. *J Med Chem*. 2014;57(19):7874–7887.
7 Zhang W, Bai Y, Wang Y, Xiao W. Polypharmacology in drug discovery: a review from systems pharmacology perspective. *Curr Pharm Des*. 2016;22(21):3171–3181.
8 Louis DN, Perry A, Wesseling P, et al. The 2021 WHO classification of tumors of the central nervous system: a summary. *Neuro Oncol*. 2021;23(8):1231–1251.
9 Brat DJ, Aldape K, Colman H, et al. cIMPACT-NOW update 3: recommended diagnostic criteria for "Diffuse astrocytic glioma, IDH-wildtype, with molecular features of glioblastoma, WHO grade IV". *Acta Neuropathol*. 2018;136(5):805–810.
10 Neftel C, Laffy J, Filbin MG, et al. An integrative model of cellular states, plasticity, and genetics for glioblastoma. *Cell*. 2019;178(4):835–849.e21.
11 Wen PY, Weller M, Lee EQ, et al. Glioblastoma in adults: a Society for Neuro-Oncology (SNO) and European Society of Neuro-Oncology (EANO) consensus review on current management and future directions. *Neuro Oncol*. 2020;22(8):1073–1113.
12 Tchoghandjian A, Baeza N, Colin C, et al. A2B5 cells from human glioblastoma have cancer stem cell properties. *Brain Pathol*. 2010;20(1):211–221.
13 Tchoghandjian A, Baeza-Kallee N, Beclin C, et al. Cortical and subventricular zone glioblastoma-derived stem-like cells display different molecular profiles and differential in vitro and in vivo properties. *Ann Surg Oncol*. 2012;19(Suppl 3):S608–S619.
14 Pasquier E, Street J, Pouchy C, et al. β-blockers increase response to chemotherapy via direct antitumour and anti-angiogenic mechanisms in neuroblastoma. *Br J Cancer*. 2013;108(12):2485–2494.
15 Zhang JH, Chung TD, Oldenburg KR. A simple statistical parameter for use in evaluation and validation of high throughput screening assays. *J Biomol Screen*. 1999;4(2):67–73.
16 Amelio I, Gostev M, Knight RA, Willis AE, Melino G, Antonov AV. DRUGSURV: a resource for repositioning of approved and experimental drugs in oncology based on patient survival information. *Cell Death Dis*. 2014;5:e1051.
17 Pacini C, Dempster JM, Boyle I, et al. Integrated cross-study datasets of genetic dependencies in cancer. *Nat Commun*. 2021;12(1):1661.
18 Louis DN, Perry A, Reifenberger G, et al. The 2016 World Health organization classification of tumors of the central nervous system: a summary. *Acta Neuropathol*. 2016;131(6):803–820.
19 Casar-Borota O, Heck A, Schulz S, et al. Expression of SSTR2a, but not of SSTRs 1, 3, or 5 in somatotroph adenomas assessed by monoclonal antibodies was reduced by octreotide and correlated with the acute and long-term effects of octreotide. *J Clin Endocrinol Metab*. 2013;98(11):E1730–E1739.
20 Ianevski A, Giri AK, Aittokallio T. SynergyFinder 3.0: an interactive analysis and consensus interpretation of multi-drug synergies across multiple samples. *Nucleic Acids Res*. 2022;50(W1):W739–W743.
21 Besse B, Olaussen KA, Soria JC. ERCC1 and RRM1: ready for prime time? *J Clin Oncol*. 2013;31(8):1050–1060.
22 Brennan CW, Verhaak RGW, McKenna A, et al. The somatic genomic landscape of glioblastoma. *Cell*. 2013;155(2):462–477.
23 Eskilsson E, Røsland GV, Solecki G, et al. EGFR heterogeneity and implications for therapeutic intervention in glioblastoma. *Neuro Oncol*. 2018;20(6):743–752.
24 Gautam A, Bepler G. Suppression of lung tumor formation by the regulatory subunit of ribonucleotide reductase. *Cancer Res*. 2006;66(13):6497–6502.
25 Zheng Z, Chen T, Li X, Haura E, Sharma A, Bepler G. DNA synthesis and repair genes RRM1 and ERCC1 in lung cancer. *N Engl J Med*. 2007;356(8):800–808.
26 Akita H, Zheng Z, Takeda Y, et al. Significance of RRM1 and ERCC1 expression in resectable pancreatic adenocarcinoma. *Oncogene*. 2009;28(32):2903–2909.
27 Gautam A, Li ZR, Bepler G. RRM1-induced metastasis suppression through PTEN-regulated pathways. *Oncogene*. 2003;22(14):2135–2142.
28 Bepler G, Sharma S, Cantor A, et al. RRM1 and PTEN as prognostic parameters for overall and disease-free survival in patients with non-small-cell lung cancer. *J Clin Oncol*. 2004;22(10):1878–1885.
29 Bepler G, Kusmartseva I, Sharma S, et al. RRM1 modulated in vitro and in vivo efficacy of gemcitabine and platinum in non-small-cell lung cancer. *J Clin Oncol*. 2006;24(29):4731–4737.
30 Yang Z, Fu B, Zhou L, Xu J, Hao P, Fang Z. RRM1 predicts clinical outcome of high-and intermediate-risk non-muscle-invasive bladder cancer patients treated with intravesical gemcitabine monotherapy. *BMC Urol*. 2019;19(1):69.
31 Chun JW, Lee B, Park WS, et al. RRM1 expression as a prognostic biomarker for unresectable or recurrent biliary tract cancer treated with gemcitabine plus cisplatin. *J Clin Med*. 2021;10(20):4652.
32 Kato T, Ono H, Fujii M, et al. Cytoplasmic RRM1 activation as an acute response to gemcitabine treatment is involved in drug

resistance of pancreatic cancer cells. *PLoS One*. 2021;16(6):e0252917.
33 Jiang K, Zhi T, Xu W, et al. MicroRNA-1468-5p inhibits glioma cell proliferation and induces cell cycle arrest by targeting RRM1. *Am J Cancer Res*. 2017;7(4):784–800.
34 Nakamizo A, Miyamatsu Y, Hirose H, et al. Metabolic remodeling of pyrimidine synthesis pathway and serine synthesis pathway in human glioblastoma. *Sci Rep*. 2022;12:16277.
35 Ferguson SD, Zheng S, Xiu J, et al. Profiles of brain metastases: prioritization of therapeutic targets. *Int J Cancer*. 2018;143(11):3019–3026.
36 Yuan Z, Yang Z, Li W, Wu A, Su Z, Jiang B. Exosome-Mediated transfer of long noncoding RNA HOTAIR regulates temozolomide resistance by miR-519a-3p/RRM1 Axis in glioblastoma. *Cancer Biother Radiopharm*. 2020;37(6):515.
37 Toledo CM, Ding Y, Hoellerbauer P, et al. Genome-wide CRISPR-cas9 screens reveal loss of redundancy between PKMYT1 and WEE1 in glioblastoma stem-like cells. *Cell Rep*. 2015;13(11):2425–2439.
38 Yin H, Xue W, Anderson DG. CRISPR–Cas: a tool for cancer research and therapeutics. *Nat Rev Clin Oncol*. 2019;16(5):281–295.
39 MacLeod G, Bozek DA, Rajakulendran N, et al. Genome-wide CRISPR-cas9 screens expose genetic vulnerabilities and mechanisms of temozolomide sensitivity in glioblastoma stem cells. *Cell Rep*. 2019;27(3):971–986.e9.
40 O'Neil J, Benita Y, Feldman I, et al. An unbiased oncology compound screen to identify novel combination strategies. *Mol Cancer Ther*. 2016;15(6):1155–1162.
41 Jaaks P, Coker EA, Vis DJ, et al. Effective drug combinations in breast, colon and pancreatic cancer cells. *Nature*. 2022;603(7899):166–173.
42 Yaeger R, Corcoran RB. Targeting alterations in the RAF-MEK pathway. *Cancer Discov*. 2019;9(3):329–341.
43 McNeill RS, Canoutas DA, Stuhlmiller TJ, et al. Combination therapy with potent PI3K and MAPK inhibitors overcomes adaptive kinome resistance to single agents in preclinical models of glioblastoma. *Neuro Oncol*. 2017;19(11):1469–1480.
44 Schreck KC, Allen AN, Wang J, Pratilas CA. Combination MEK and mTOR inhibitor therapy is active in models of glioblastoma. *Neurooncol Adv*. 2020;2(1):vdaa138.
45 Pilié PG, Tang C, Mills GB, Yap TA. State-of-the-art strategies for targeting the DNA damage response in cancer. *Nat Rev Clin Oncol*. 2019;16(2):81–104.
46 Hirose Y, Berger MS, Pieper RO. Abrogation of the Chk1-mediated G(2) checkpoint pathway potentiates temozolomide-induced toxicity in a p53-independent manner in human glioblastoma cells. *Cancer Res*. 2001;61(15):5843–5849.
47 Aasland D, Götzinger L, Hauck L, et al. Temozolomide induces senescence and repression of DNA repair pathways in glioblastoma cells via activation of ATR-CHK1, p21, and NF-κB. *Cancer Res*. 2019;79(1):99–113.
48 Dai Y, Chen S, Pei XY, et al. Interruption of the Ras/MEK/ERK signaling cascade enhances Chk1 inhibitor-induced DNA damage in vitro and in vivo in human multiple myeloma cells. *Blood*. 2008;112(6):2439–2449.
49 Tang Y, Dai Y, Grant S, Dent P. Enhancing CHK1 inhibitor lethality in glioblastoma. *Cancer Biol Ther*. 2012;13(6):379–388.
50 Ando K, Ohira M, Takada I, et al. FGFR2 loss sensitizes MYCN-amplified neuroblastoma CHP134 cells to CHK1 inhibitor-induced apoptosis. *Cancer Sci*. 2022;113(2):587–596.
51 Berdasco M, Esteller M. Aberrant epigenetic landscape in cancer: how cellular identity goes awry. *Dev Cell*. 2010;19(5):698–711.
52 Stathis A, Bertoni F. BET proteins as targets for anticancer treatment. *Cancer Discov*. 2018;8(1):24–36.
53 Morel D, Jeffery D, Aspeslagh S, Almouzni G, Postel-Vinay S. Combining epigenetic drugs with other therapies for solid tumours - past lessons and future promise. *Nat Rev Clin Oncol*. 2020;17(2):91–107.
54 Enßle JC, Boedicker C, Wanior M, Vogler M, Knapp S, Fulda S. Co-targeting of BET proteins and HDACs as a novel approach to trigger apoptosis in rhabdomyosarcoma cells. *Cancer Lett*. 2018;428:160–172.
55 Zhang X, Zegar T, Weiser T, et al. Characterization of a dual BET/HDAC inhibitor for treatment of pancreatic ductal adenocarcinoma. *Int J Cancer*. 2020;147(10):2847–2861.
56 Kling MJ, Kesherwani V, Mishra NK, et al. A novel dual epigenetic approach targeting BET proteins and HDACs in Group 3 (MYC-driven) Medulloblastoma. *J Exp Clin Cancer Res*. 2022;41(1):321.
57 Liu T, Wan Y, Xiao Y, Xia C, Duan G. Dual-target inhibitors based on HDACs: novel antitumor agents for cancer therapy. *J Med Chem*. 2020;63(17):8977–9002.
58 Gusyatiner O, Bady P, Pham MDT, et al. BET inhibitors repress expression of interferon-stimulated genes and synergize with HDAC inhibitors in glioblastoma. *Neuro Oncol*. 2021;23(10):1680–1692.
59 Felgenhauer J, Tomino L, Selich-Anderson J, Bopp E, Shah N. Dual BRD4 and AURKA inhibition is synergistic against MYCN-amplified and nonamplified neuroblastoma. *Neoplasia*. 2018;20(10):965–974.
60 Yi JS, Sias-Garcia O, Nasholm N, et al. The synergy of BET inhibitors with aurora A kinase inhibitors in MYCN-amplified neuroblastoma is heightened with functional TP53. *Neoplasia*. 2021;23(6):624–633.
61 Čančer M, Drews LF, Bengtsson J, et al. BET and Aurora Kinase A inhibitors synergize against MYCN-positive human glioblastoma cells. *Cell Death Dis*. 2019;10(12):881.
62 Stathias V, Jermakowicz AM, Maloof ME, et al. Drug and disease signature integration identifies synergistic combinations in glioblastoma. *Nat Commun*. 2018;9(1):5315.
63 Wong CH, Siah KW, Lo AW. Estimation of clinical trial success rates and related parameters. *Biostatistics*. 2019;20(2):273–286.
64 Honkala A, Malhotra SV, Kummar S, Junttila MR. Harnessing the predictive power of preclinical models for oncology drug development. *Nat Rev Drug Discov*. 2022;21(2):99–114.
65 Wellbourne-Wood J, Chatton JY. From cultured rodent neurons to human brain tissue: model systems for pharmacological and translational neuroscience. *ACS Chem Neurosci*. 2018;9(8):1975–1985.
66 Song A, Andrews DW, Werner-Wasik M, et al. Phase I trial of alisertib with concurrent fractionated stereotactic re-irradiation for recurrent high grade gliomas. *Radiother Oncol*. 2019;132:135–141.